# Weierstraß-Institut
## für Angewandte Analysis und Stochastik

im Forschungsverbund Berlin e.V.

Preprint ISSN 0946 – 8633


# Stress analysis and bending tests for GaAs wafer


Wolfgang Dreyer[1], Frank Duderstadt[1],

Stefan Eichler[2], Manfred Jurisch[2]



submitted: 14th December 2003



[1] Weierstrass Institute
for Applied Analysis and Stochastics
Mohrenstraße 39
D – 10117 Berlin
Germany
E-Mail: dreyer@wias-berlin.de
E-Mail: dudersta@wias-berlin.de

[2] Freiberger Compound Materials GmbH

Am Junger Löwe Schacht 5
D – 09599 Freiberg / Sachsen
Germany
E-Mail: eichler@fcm-germany.com
E-Mail: jurisch@fcm-germany.com



No. 897
Berlin 2003




2000 *Mathematics Subject Classification.* 74B2, 74K20, 74M20, 74M15.

*Key words and phrases.* non-linear elasticity, anisotropy, plate theory, von Kármán, Hertzian contact.

Edited by
Weierstraß-Institut für Angewandte Analysis und Stochastik (WIAS)
Mohrenstraße 39
10117 Berlin
Germany

Fax: + 49 30 2044975
E-Mail: preprint@wias-berlin.de
World Wide Web: http://www.wias-berlin.de/

**Abstract**

Wafer made from single crystal Gallium Arsenide (GaAs) are used as substrate materials in micro- and opto- electronic devices. During the various processes of manufacturing, the wafer are subjected to mechanical loads which may lead to fracture. The characterization of the fracture strength of the wafer needs bending tests and a theoretical calculation of various stress distributions within the wafer.

In this study we show that the nonlinear *von Kármán* theory may serve as an appropriate tool to calculate the stress distributions as functions of the external load, while the *Kirchhoff* theory has turned out to be completely inappropriate. Our main focus is devoted to (*i*) calculation of the contact area between the load sphere and the wafer, (*ii*) study of the influence of the anisotropic character of the material, (*iii*) study of the important geometric nonlinearity. Finally we compare the calculated and theoretical load-flexure relations in order to demonstrate the high accuracy of the *von Kármán* theory and its Finite Element implementation.

# 1 Introduction

## 1.1 Objective of this study

The lower fracture toughness $K_{IC} = 0.45$ MPa $m^{1/2}$ of GaAs [1] compared to 0.82 - 0.95 MPa $m^{1/2}$ for silicon [2] makes this brittle material significantly more susceptible to wafer breakage during handling procedures in device manufacturing and, therefore, to one of the factors determining the yield of devices. Wafer breakage is caused by the existence or nucleation of defects acting as crack nuclei and their uncontrolled growth during loading. Due to the low fracture toughness of GaAs already crack nuclei of submicroscopic size like surface or subsurface defects are of relevance. The propensity to cracking may further increase due to structural defects like localized dislocation clusters, As-precipitates or residual stresses.

Crack nuclei can be generated either during the automatic or manual handling possibly accomplished by a shock-like loading due to liners or chucks and leading to defects like scratches or are already present in the wafers. Therefore, it is essential to separate wafer breakage as a result of an unproper handling from that of wafer quality.

This requires a wafer breakage test which gives reliable estimates of fracture strength and, furthermore, can be applied as a basis to control relevant technological steps

during crystal growth and wafer preparation such as annealing, sawing, grinding, damage etching and polishing.

The disc bending is used based on the double-ring loading set-up according to *DIN EN* 1288-5: 2000 [9] and modified in that [13] a small diameter ball (1/8 inches) replaces the ring for centrally loading the wafer (see also [6]). As wafer bending at fracture is much greater than wafer thickness linear approaches were expected to be inappropriate to describe the load - displacement behaviour and to calculate the maximum surface stresses at fracture. Therefore, FEM analysis of the test arrangement were performed allowing for large displacements.

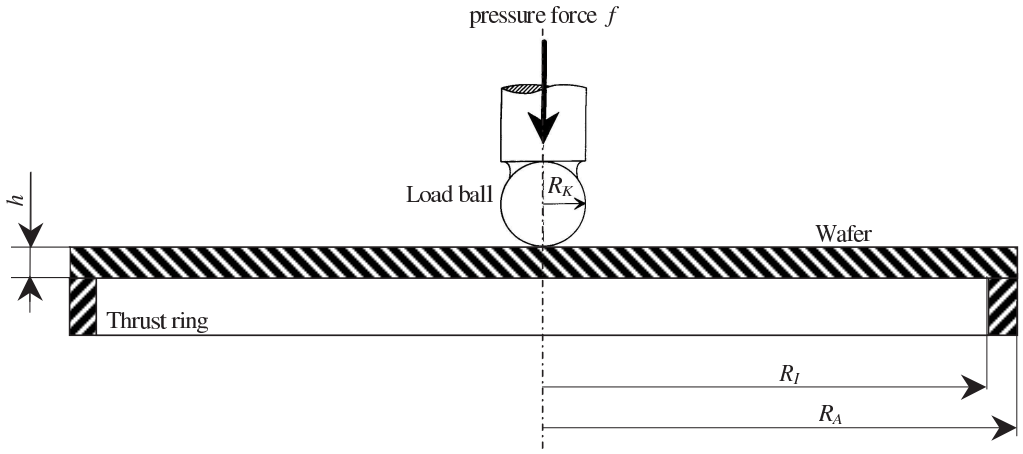


Figure 1: Principle drawing of the test after *Hu* [6].

We describe now in detail the fracture test of a thin circular wafer. Figure 1 shows the principle drawing of the device. During the test, the wafer lies concentrically on the double ring. The load $f$ is applied by a steel ball. The objective of this study is the calculation of the distribution of the resulting stresses, because these are not measurable directly. The measurable quantities are the displacements and the applied loads.

The calculation of displacements, strains and stresses rely on the following assumptions:

- The GaAs wafer is a cubic anisotropic material, whose [001] direction is parallel to the load axis.
- The load supply by means of a steel ball induces a contact area on the wafer, which is calculated according to *Hertz* theory for an isotropic ball on a cubic anisotropic half space. The half space is oriented so that its normal coincides with the [001] direction. Furthermore, the *Hertz* theory yields the pressure distribution on the contact area.
- The hollow cylinder, which establishes the support ring, is assumed to be rigid.

- The contact line between the wafer and the support ring remains circular with radius $R_I$. Along the contact line the wafer may freely rotate and can freely be displaced in horizontal direction. The vertical displacement along the contact line is assumed to be zero.

## 1.2 The mechanical model

In order to calculate stresses and displacements, we simplify the original 3D problem by reducing the 3D model of elasticity to a 2D model which is appropriate fort thin plates. The 2D model yields approximate solutions, that converge to the solutions of the original 3D problem in the limiting case of an infinitely thin plate. A 2D plate theory is superior to the 3D problem, because a precise calculation of the deformation of a cylinder whose height is small with respect to its diameter requires a tremendous numerical effort.

The 2D plate theory which is used here, is the *von Kármán* theory [7, 3], which is valid for small and moderate deflections. The technical terms small and moderate have the following meaning: We call a deflection small, if it is small with respect to the plate thickness, while moderate deflections may be several times larger as the thickness, but they are understood to be still small with respect to the plate diameter. In this respect we call a deflection large, if it is comparable with the plate diameter. The well known plate theory according to *Kirchhoff* is the linearized version of the *von Kármán* theory. The Kirchhoff theory is appropriate if the deflection is small. Within the *Kirchhoff* theory, membrane and bending effects are decoupled, while they are strongly coupled in the *von Kármán* Theory.

We consider a plate, whose middle surface is a plane in its stress free state. If an external load leads to a curved but not dilated middle surface, the deformation of the plate is called pure bending. The layers above and below the middle surface are compressed and elongated, respectively. Elastic materials resist to these deformations and respond with bending stresses. The resistance is called bending stiffness. Continua without bending stiffness are called flabby. Pure membrane stresses appear due to straining of the middle surface. The resistance of an elastic plate against such strain is called membrane stiffness. If the membrane stress is much larger than the maximal bending stress, we may neglect the bending stress. Theories that neglect bending stresses right at the very beginning, are called membrane theories. They are especially applied for large flexures. The *von Kármán* theory describes the deformation appropriately if both effects appear simultaneously, and this happens in the test under consideration.

Finally we discuss the difference between *Reissner-Mindlin* plate theories [10, 8], which are also often used, and the von Kármán theory. As it was already explained, the von Kármán theory is the 2D limiting case of conventional 3D elasticity theory, i.e. the 3D start is the conventional *Hooke*'s law. In contrast, the *Reissner-Mindlin* plate theories do not rely on conventional elasticity theory, but their derivation starts from a *Cosserat* model [4].

Approximative solutions of the boundary value problem for the *von Kármán* theory relies on its weak formulation. The corresponding variational principle results from the introduction of virtual displacements, and we use the method of finite elements for its exploitation. To this end we establish a 2D finite element triangulation of the middle surface of the plate. The higher order triangle elements are based on an ansatz with pure displacements.

### 1.3 Load range and material data

The calculations are made for a wafer with the diameter $2R_A = 150$ mm, and the thicknesses is $h = 0.675$ mm. The applied load ranges from 0 to 600 N. The inner diameter of the support ring is $2R_I = 142$ mm. The load is supplied by a steel ball, whose diameter is $2R_K = 1/8" = 3.175$ mm. At 300 K the *Voigt* constants of the wafer material are: $c_{11} = (119.0 \pm 0.1)$ GPa, $c_{12} = (53.8 \pm 0.1)$ GPa, $c_{44} = (59.5 \pm 0.1)$ GPa. Young modulus and Poisson number for the steel ball are given as $E_S = 210$ GPa and $\nu_S = 0.3$ .

## 2 A modicum of the theory of elasticity

### 2.1 Description of the deformation

We consider an elastic solid body which occupies the space $\Omega_0 \subset \mathbb{R}^3$ in the stress free configuration. Here we identify the material particles of the body by its coordinates $\boldsymbol{X} = (X_1, X_2, X_3)$ with respect to a cartesian coordinate system. The deformed body occupies the space $\Omega \subset \mathbb{R}^3$, and a particle with coordinates $\boldsymbol{X} = (X_1, X_2, X_3)$ in the stress free configuration has now the cartesian coordinates $\boldsymbol{x} = (x_1, x_2, x_3)$. The function $\boldsymbol{\chi} : \Omega_R \to \Omega$, which maps the coordinates $\boldsymbol{X}$ to $\boldsymbol{x}$ , is called motion. We write

$$x_i = \chi_i(X_1, X_2, X_3) \quad \text{for} \quad i = 1, 2, 3 \ . \tag{1}$$

The quality of central importance for the description of the change of placement is the deformation gradient

$$F_{ij} = \frac{\partial \chi_i}{\partial X_j} \quad \text{with the property} \quad J = \det(\boldsymbol{F}) > 0. \tag{2}$$

In the reference configuration we have $F_{ij} = \delta_{ij}$, where $\delta_{ij}$ denotes the components of the unit matrix. A given deformation can be decomposed into a rigid body rotation and a stretching. The stretching contains the strain. The strain is zero for a pure rigid body motion. It is a known fact, that the strain exclusively gives rise to stresses. A possible measure of the stretching is given by the combination $F_{ki}F_{kj}$. In the following we only consider the case, that the strain is small, but the rigid body rotation might be quite large. As the measure of strain we introduce the so

called *Green* strain tensor, which is defined by

$$G_{ij} = (F_{ki}F_{kj} - \delta_{ij})/2 \ . \tag{3}$$

The actual position of a material particle at the location $\boldsymbol{X}$ in the reference configuration is conveniently be described by the displacement vector $u_i$, according to

$$u_i(X_1, X_2, X_3) = \chi_i(X_1, X_2, X_3) - X_i \tag{4}$$

so that now the deformation gradient and the Green strain tensor, respectively read

$$F_{ij} = \delta_{ij} + \frac{\partial u_i}{\partial X_j} \tag{5}$$

and

$$G_{ij} = \frac{1}{2}\left(\frac{\partial u_i}{\partial X_j} + \frac{\partial u_j}{\partial X_i} + \frac{\partial u_k}{\partial X_i}\frac{\partial u_k}{\partial X_j}\right). \tag{6}$$

## 2.2 Stresses

There are three different measures of stress, viz.

| | | |
|---|---|---|
| $t_{ij}$ | – | *Cauchy* stress |
| $T_{ij} = Jt_{ir}(F^{-1})_{jr}$ | – | *Piola - Kirchhoff* stress of the $1^{th}$ kind, |
| $\sigma_{ij} = J(F^{-1})_{is}t_{sr}(F^{-1})_{jr}$ | – | *Piola - Kirchhoff* stress of the $2^{nd}$ kind. |

The three stresses have different meanings: The *Cauchy* stresses, which are also called true stresses, give the actual forces with respect to the actual area, while the $1^{th}$ *Piola-Kirchhoff* stresses give the actual force with respect to the corresponding area of the reference configuration. The $2^{nd}$ *Piola-Kirchhoff* stresses live with both indices in the reference configuration, i.e. also the forces are here transformed to the reference configuration, so that material symmetries, if there are any, can conveniently incorporated.

The mechanical equilibrium conditions form the basic equations for the calculation of the deformation. They may be written alternatively either

$$\frac{\partial t_{ik}}{\partial x_k} = 0 \quad \text{in actual coordinates, or} \quad \frac{\partial T_{ik}}{\partial X_k} = 0 \quad \text{in reference coordinates.} \tag{7}$$

Furthermore there is a third alternative, viz. $\frac{\partial F_{ij}\sigma_{jk}}{\partial X_k} = 0$ and by means of (5)

$$\frac{\partial}{\partial X_k}\left(\sigma_{ik} + \frac{\partial u_i}{\partial X_j}\sigma_{jk}\right) = 0. \tag{8}$$

The derivation of the plate theory according to *von Kármán* relies on the version (8).

## 2.3 The constitutive law of *St-Venant – Kirchhoff*

The constitutive law of *St-Venant – Kirchhoff* postulates a linear and homogeneous relation between the $2^{nd}$ *Piola – Kirchhoff* stress and the *Green* strain, and restricts its applicability to small strains. However, note that rigid body rotations are still allowed to be arbitrary large, see [11] for more details. The linearisation of the *St-Venant – Kirchhoff* law with respect to the displacement gradient $\frac{\partial u_i}{\partial X_j}$ leads to the well known *Hooke* law. Its applicability requires also small rigid body rotation. The *St-Venant – Kirchhoff* law reads

$$\sigma_{ij} = C_{ijmn} G_{mn}, \quad \text{and} \quad G_{ij} = S_{ijmn}\sigma_{mn} \quad \text{with} \tag{9}$$

$$C_{ijmn} S_{mnkl} = (\delta_{ik}\delta_{jl} + \delta_{il}\delta_{jk})/2, \quad \text{respectively.} \tag{10}$$

The newly introduced quantities $C_{ijmn}$ and $S_{ijmn}$ denote the stiffness tensor and the compliance, respectively.

Single crystal GaAs has cubic symmetry in the reference configuration. If we introduce now a coordinate system that coincides with the three crystal axes, there holds

$$C_{ijmn} = \lambda\ \delta_{ij}\delta_{mn} + \mu(\delta_{im}\delta_{jn} + \delta_{in}\delta_{jm}) + \mu'\ \delta_{ijmn}. \tag{11}$$

The material constants $\lambda$ and $\mu$ are called *Lamé* constants. The quantity $\delta_{ijmn}$ is defined by $\delta_{1111} = \delta_{2222} = \delta_{3333} = 1$ and $\delta_{ijmn} = 0$ otherwise. The appearance of the constant $\mu'$ reflects the 90° symmetry of the cubic crystal, while we have $\mu' = 0$ in the isotropic body. The constants $\lambda$, $\mu$ and $\mu'$ may be related to the so called *Voigt* constants, which are more frequently used, according to

$$\mu = c_{44}, \quad \lambda = c_{12} \quad \text{and} \quad \mu' = c_{11} - c_{12} - 2c_{44}. \tag{12}$$

The inverse of the stiffness matrix, which is called compliance, has the representation

$$S_{ijmn} = s_{12}\delta_{ij}\delta_{mn} + s_{44}(\delta_{im}\delta_{jn} + \delta_{in}\delta_{jm}) + (s_{11} - s_{12} - s_{44}/2)\delta_{ijmn}, \tag{13}$$

and we calculate the relations

$$s_{12} = \frac{c_{12}}{(2c_{12} + c_{11})(c_{11} - c_{12})}, \quad s_{44} = \frac{1}{c_{44}} \quad \text{and} \quad s_{11} = -s_{12}\left(1 + \frac{c_{11}}{c_{12}}\right). \tag{14}$$

## 2.4 The boundary conditions

We describe the plate with respect to a cartesian coordinate system, whose origin lies in the center of the middle plane. The $X_1$- and $X_2$-axis are lying in the middle plane and are parallel to the $\{100\}$-plane. The $X_3$-axis is perpendicular to the middle plane and points downwards. We have thus fixed that the 3-component of the displacement, $u_3$, measures the actual flexure of the plate, while the two other components give its horizontal displacements.

In order to formulate the boundary conditions some further notations are needed. According to the described device from Figure 1, we denote the middle plane of the cylinder $\Omega_0$ by $\omega_0$. Its boundary $\partial\omega_0$ is contained in the exterior cylinder $\Gamma_0 = \partial\omega_0 \times [-h/2, h/2]$ with radius $R_A$. The lower and upper surface of the cylinder are denoted by $\partial\Omega_{0-} = \omega_0 \times \{-h/2\}$ and $\partial\Omega_{0+} = \omega_0 \times \{h/2\}$, respectively. The inner edge of the support ring generates the line $S_0 \in \partial\Omega_{0+}$

$$S_0 = \{(X_1, X_2, X_3) \mid (\chi_1(X_1, X_2, h/2))^2 + (\chi_2(X_1, X_2, h/2))^2 = R_I^2, X_3 = h/2\}. \tag{15}$$

It will turn out later on that $S_0$ is approximately a circle with radius $R_I$. Finally we introduce the exterior normals and the tangent vectors $\boldsymbol{n} = (n_1, n_2, 0)$ and $\boldsymbol{s} = (-n_2, n_1, 0)$, respectively, at the locations $\boldsymbol{X} \in \Gamma_0$.

For the evaluation of the equilibrium conditions we prevent horizontal rigid body motions within the middle plane of the plate by the locations

$$P_{0O}, P_{0N}, P_{0W} \in \omega_0 \times \{0\} \subset \Gamma_0 \quad \text{with} \quad P_{0O} = (R_A, 0, 0),\ P_{0N} = (0, R_A, 0) \quad \text{and} \quad P_{0W} = (-R_A, 0, 0). \tag{16}$$

The boundary conditions read for $i \in \{1, 2, 3\}$ and $\alpha \in \{1, 2\}$

$$\begin{aligned}
T_{ij} n_j &= 0 \quad \text{on} \quad \Gamma_0 \quad \text{except in } P_{0O}, P_{0N}, P_{0W} && (17)\\
T_{3j} n_j &= 0 \quad \text{in} \quad P_{0O}, P_{0N}, P_{0W}, && (18)\\
u_j s_j &= 0 \quad \text{in} \quad P_{0O}, P_{0N}, P_{0W}, && (19)\\
T_{11} &= 0 \quad \text{in} \quad P_{0O} \text{ and } P_{0W} \quad \text{as well as} \quad T_{22} = 0 \quad \text{in} \quad P_{0N}, && (20)\\
T_{\alpha 3} &= 0 \quad \text{on} \quad \partial\Omega_{0+}, && (21)\\
\sigma_{\alpha 3} &= 0 \quad \text{on} \quad \partial\Omega_{0-}, && (22)\\
\sigma_{33} &= -p(X_1, X_2) \quad \text{on} \quad \partial\Omega_{0-}, && (23)\\
\sigma_{33} &= 0 \quad \text{on} \quad \partial\Omega_{0+} \quad \text{except on} \quad S_0 \quad \text{and} && (24)\\
u_3 &= 0 \quad \text{on} \quad S_0. && (25)
\end{aligned}$$

Recall that we use the equilibrium conditions with respect to reference coordinates, which implies that the stress boundary conditions must be formulated for the *Piola - Kirchhoff* stresses of the $1^{th}$ kind.

# 3 A modicum of the theory of plates

According to Figure 1 we consider cylindrical plates with thickness $h$ and with radius $R_A$. Thin plates are characterized by the restriction $h/(2R_A) \ll 1$. The objective of the elasticity theory of thin plates is the reduction of the original 3D plate problem to a 2D plate problem. To this end the field of deformation as well as the constitutive law and the equilibrium conditions must be properly reduced.

## 3.1 The deformation of thin plates

The deformation field of the plate theory according to von Kármán relies on five restrictions, which are: We take care explicitly for the restriction

(i)
$$h \ll 2R_A$$

to simplify the deformation field. Furthermore we consider exclusively deformations, so that there holds

(ii)
$$|G_{ij}| \ll 1.$$

The horizontal components of the displacement is restricted to

(iii)
$$|u_\alpha| \ll h \quad \text{for} \quad \alpha = 1, 2, \tag{26}$$

while the flexure must satisfy

(iv)
$$|u_3| \ll 2R_I. \tag{27}$$

Thus only small deformations and small rotations are allowed within the horizontal plane. However, flexures and the corresponding rotations out of the middle plane might be moderate large, i.e. flexures might be several times larger as the plate thickness, but they are understood to be still small with respect to the plate diameter.

Finally we need the assumption that we may set

(v)
$$\frac{\partial u_i}{\partial X_3} + \frac{\partial u_3}{\partial X_i} = 0 \tag{28}$$

for thin plates. This assumption, however, is only needed in the following intuitive derivation of the *von Kármán* theory, whereas the assumption (v) results in a rigorous derivation by means of asymptotic expansions. The evaluation of (28) exhibits the equivalence of (28) with the often used *Bernoulli* hypothesis, whereupon planes which lie perpendicular to the middle plane in the undeformed configuration remain perpendicular after deformation.

Next we will show that displacements satisfying the condition (28) can only depend linearly on $X_3$, and it is thus sufficient to determine the displacements of the middle surface $u_i(X_1, X_2, 0)$ in order to calculate the total displacements $u_i(X_1, X_2, X_3)$. To this end we start with the evaluation of (28) for $i = 3$. We conclude from the condition

$$u_3(X_1, X_2, X_3) = W(X_1, X_2). \tag{29}$$

The evaluation of (28) for $i = \alpha$, viz. $\frac{\partial u_\alpha}{\partial X_3} + \frac{\partial u_3}{\partial X_\alpha} = 0$, yields by means of (29)

$$u_\alpha(X_1, X_2, X_3) = U_\alpha(X_1, X_2) - X_3 \frac{\partial W(X_1, X_2)}{\partial X_\alpha}. \tag{30}$$

The functions $U_1,\ U_2$ and $W$ depend only on $X_1$ and $X_2$. We evaluate (29) and (30) on the surface $X_3 = 0$ , and obtain

$$u_\alpha(X_1, X_2, 0) = U_\alpha(X_1, X_2) \quad \text{and} \quad u_3(X_1, X_2, 0) = W(X_1, X_2). \tag{31}$$

Consequently we may interpret the functions $U_\alpha$ and $W$ as displacements of the middle surface. Note that the function $u_3$ does not depend on $X_3$. From this follows that $W(X_1, X_2)$ additionally gives the displacements of each material point from the line $\{X_1\}\times\{X_2\} \times [-h/2, h/2]$ in the direction $X_3$.

Regarding the $\alpha\beta$-components of the *Green* strain tensor, we obtain according to (3) and by means (29) and (30) the representation

$$G_{\alpha\beta} = \frac{1}{2}\left(\frac{\partial U_\alpha}{\partial X_\beta} + \frac{\partial U_\beta}{\partial X_\alpha} - 2X_3 \frac{\partial^2 W}{\partial X_\alpha \partial X_\beta} + \frac{\partial W}{\partial X_\alpha}\frac{\partial W}{\partial X_\beta}\right). \tag{32}$$

***Remark***: The linearisation of $G_{ij}$ and of the $1^{th}$ Piola-Kirchhoff stress and the $2^{nd}$ *Piola - Kirchhhoff* stress leads to the linear theory of elasticity. The corresponding plate theory is the *Kirchhoff* theory, that relies on the *Kirchhoff-Love* displacement field according to (28).

## 3.2 The *St-Venant – Kirchhoff* law for thin plates

In order to derive a 2D constitutive law for thin plates, we start from corresponding 3D (9). In $\langle 100\rangle$-Orientation the $G_{\alpha\beta}$ components of the *Green* strain read

$$G_{\alpha\beta} = s_{12}\delta_{\alpha\beta}(\sigma_{\gamma\gamma} + \sigma_{33}) + 2s_{44}\sigma_{\alpha\beta} + (s_{11} - s_{12} - s_{44}/2)\delta_{\alpha\beta}\sigma_{\underline{\beta\beta}}. \tag{33}$$

Underlined indices indicate that the summation rule will not be applied.

The stress field of the plate theory according to *von Kármán* relies on two restrictions, which are:

(vi) $$|\sigma_{33}| \ll \|\sigma_{\alpha 3}\| \quad \text{and}$$

(vii) $$|\sigma_{\alpha 3}| \ll \|\sigma_{\alpha\beta}\| \quad \text{for } \alpha = 1, 2.$$

If we assume that $\sigma_{33}$ may be ignored with respect to $\sigma_{\gamma\gamma}$, the representation (33) reduces to a pure 2D representation of the strain:

$$G_{\alpha\beta} = s_{12}\delta_{\alpha\beta}\sigma_{\gamma\gamma} + 2s_{44}\sigma_{\alpha\beta} + (s_{11} - s_{12} - s_{44}/2)\delta_{\alpha\beta}\sigma_{\underline{\beta\beta}}. \tag{34}$$

The inverse of this equation reads

$$\sigma_{\alpha\beta} = \lambda \frac{2\mu + \mu'}{2\mu + \mu' + \lambda} \delta_{\alpha\beta} G_{\gamma\gamma} + 2\mu G_{\alpha\beta} + \mu' \delta_{\alpha\beta} G_{\underline{\beta\beta}}. \tag{35}$$

and gives the 2D *St-Venant – Kirchhoff* law of the plane stress.

The description of the displacement field of the plate, $u_i$, by the displacements $U_a$ and $W$ of the middle surface implies at first an overdetermined system of field equations, because a part of its solution is taken from outside the model. Such a case is not unusual and can be resolved as follows. According to the above we relate only the components $\sigma_{\alpha\beta}$ of the stress. Hereafter integrate the remaining components $\sigma_{\alpha 3}$ and $\sigma_{33}$ over the thickness of the plate, and add the resulting expressions to the list of the unknown variables. After having solved the reduced boundary value problem, we calculate the components $\sigma_{\alpha 3}$ and $\sigma_{33}$ by means of the remaining fields equations and the boundary conditions for the stresses.

## 3.3 Evaluation of the equilibrium conditions for thin plates

We now consider in detail the equilibrium conditions (7) and (8) to obtain also here a reduction of the original 3D to a 2D problem. To this end we calculate at first the leading order terms of the $1^{th}$ *Piola - Kirchhoff* stresses and assume that $\sigma_{\alpha 3}$ and $\sigma_{33}$ can be ignored with respect to $\sigma_{\alpha\beta}$ and $\sigma_{\alpha 3}$, respectively

$$\boldsymbol{T} = \boldsymbol{\sigma} + \begin{pmatrix} 0 & 0 & 0 \\ 0 & 0 & 0 \\ \frac{\partial W}{\partial X_1}\sigma_{11} + \frac{\partial W}{\partial X_2}\sigma_{12} & \frac{\partial W}{\partial X_1}\sigma_{12} + \frac{\partial W}{\partial X_2}\sigma_{22} & \frac{\partial W}{\partial X_1}\sigma_{13} + \frac{\partial W}{\partial X_2}\sigma_{23} \end{pmatrix}. \tag{36}$$

Next we write the equilibrium conditions $\frac{\partial T_{ij}}{\partial X_j} = 0$ as $\frac{\partial T_{\alpha\beta}}{\partial X_\beta} + \frac{\partial T_{\alpha 3}}{\partial X_3} = 0$, and $\frac{\partial T_{3\beta}}{\partial X_\beta} + \frac{\partial T_{33}}{\partial X_3} = 0$, respectively, and we substitute the quantities $T_{i3}$ by their corresponding counterparts from (36). We obtain finally

$$\frac{\partial \sigma_{\alpha\beta}}{\partial X_\beta} + \frac{\partial \sigma_{\alpha 3}}{\partial X_3} = 0 \quad \text{and} \quad \frac{\partial \sigma_{3\beta}}{\partial X_\beta} + \frac{\partial}{\partial X_\beta}\left(\frac{\partial W}{\partial X_\alpha}\sigma_{\alpha\beta}\right) + \frac{\partial S_{33}}{\partial X_3} = 0. \tag{37}$$

Now we introduce those suggestive quantities, which are of central importance within the theory of plates:

$$N_{\alpha\beta}(X_1, X_2) := \int_{-h/2}^{h/2} \sigma_{\alpha\beta}(X_1, X_2, X_3) \mathrm{d}X_3 \quad — \quad \text{stress resultants,} \tag{38}$$

$$M_{\alpha\beta}(X_1, X_2) := \int_{-h/2}^{h/2} \sigma_{\alpha\beta}(X_1, X_2, X_3) X_3 \mathrm{d}X_3 \quad — \quad \text{stress couples,} \tag{39}$$

$$Q_{\alpha}(X_1, X_2) := \int_{-h/2}^{h/2} \sigma_{\alpha 3}(X_1, X_2, X_3) \mathrm{d}X_3 \quad — \quad \text{shear force.} \tag{40}$$

Stress resultants and shear stress resultants a equipped with the physical dimension force per line, while the stress couples have the dimension of a force. All these quantities appear, when we integrate the equilibrium conditions (37) over the thickness of the plate. At first we obtain from $(37)_1$

$$\int_{-h/2}^{h/2} \frac{\partial \sigma_{\alpha\beta}(X_1, X_2, X_3)}{\partial X_\beta} \mathrm{d}X_3 + \sigma_{\alpha 3}(X_1, X_2, h/2) - \sigma_{\alpha 3}(X_1, X_2, -h/2) = 0$$

and consider the boundary conditions (21) and (22) to obtain

$$\frac{\partial N_{\alpha\beta}}{\partial X_\beta} = 0 \quad \text{in} \quad \omega_0. \tag{41}$$

The corresponding integration of $(37)_2$ yields by means of the boundary conditions (23) through (25)

$$\frac{\partial}{\partial X_\beta}\left(Q_\beta + \frac{\partial W}{\partial X_\alpha} N_{\alpha\beta}\right) = -p \quad \text{for all} \quad (X_1, X_2) \in \omega_0 \quad \text{and} \quad (X_1, X_2, h/2) \notin S_0. \tag{42}$$

Next we multiply $(37)_1$ by $X_3$, and integrate over the thickness to obtain by means of the boundary conditions (21) and (22)

$$\frac{\partial M_{\alpha\beta}}{\partial X_\beta} = Q_\alpha \quad \text{in} \quad \omega_0. \tag{43}$$

Now we substitute $Q_\alpha$ in (42) by means of (43) and obtain

$$\frac{\partial^2 M_{\alpha\beta}}{\partial X_\alpha \partial X_\beta} + \frac{\partial^2 W}{\partial X_\alpha \partial X_\beta} N_{\alpha\beta} = -p \quad \text{for all} \quad (X_1, X_2) \in \omega_0 \quad \text{and} \quad (X_1, X_2, h/2) \notin S_0. \tag{44}$$

Finally we relate the resultants to the displacements, so that the equations of the system (41) and (44) become the *von Kármán* field equations for the unknown displacements.

The relations between resultants and displacements result in two steps. We insert the 2D *St-Venant – Kirchhoff* law (35) into the definitions (38) and (39). Hereafter we take for the explicit dependence on explizite $X_3$ according to representation (32). and integrate again over the thickness. There follows

$$\int_{-h/2}^{h/2} G_{\alpha\beta}(X_1, X_2, X_3) \mathrm{d}X_3 = h\ G_{\alpha\beta}(X_1, X_2, 0)$$

$$= \frac{h}{2}\left(\frac{\partial U_\alpha(X_1, X_2)}{\partial X_\beta} + \frac{\partial U_\beta(X_1, X_2)}{\partial X_\alpha} + \frac{\partial W(X_1, X_2)}{\partial X_\alpha}\frac{\partial W(X_1, X_2)}{\partial X_\beta}\right) \tag{45}$$

and

$$\int_{-h/2}^{h/2} G_{\alpha\beta}(X_1, X_2, X_3) X_3 \mathrm{d}X_3 = -\frac{h^2}{12} \frac{\partial^2 W(X_1, X_2)}{\partial X_\alpha \partial X_\beta}. \tag{46}$$

With $G^0_{\alpha\beta}(X_1, X_2) := G_{\alpha\beta}(X_1, X_2, 0)$ we obtain the components of the stress resultants

$$N_{\alpha\beta} = h \left( \lambda \frac{2\mu + \mu'}{2\mu + \mu' + \lambda} G^0_{\gamma\gamma} \delta_{\alpha\beta} + 2\mu G^0_{\alpha\beta} + \mu' \delta_{\alpha\beta} G^0_{\underline{\beta}\underline{\beta}} \right) \tag{47}$$

and the stress couples, respectively,

$$M_{\alpha\beta} = -\frac{h^3}{12} \left( \lambda \frac{2\mu + \mu'}{2\mu + \mu' + \lambda} \frac{\partial^2 W}{\partial X_\gamma \partial X_\gamma} \delta_{\alpha\beta} + 2\mu \frac{\partial^2 W}{\partial X_\alpha \partial X_\beta} + \mu' \delta_{\alpha\beta} \frac{\partial^2 W}{\partial X_{\underline{\beta}} \partial X_{\underline{\beta}}} \right). \tag{48}$$

The three equations (41) and (44), and the constitutive laws (47) and (48) will now be supplemented by boundary conditions and the given pressure load $p(X_1, X_2)$ in order to obtain the field equations of the *von Kármán* plate theory for the unknown displacements $U_\alpha(X_1, X_2)$ and $W(X_1, X_2)$. In Section 3 we will use the *Hertz* pressure theory in order to calculate $p(X_1, X_2)$ for a given external force $f$. The necessary 2D boundary conditions rely on the 3D boundary conditions respectively (17) through (25). Their derivation is the subject of the next subsection.

## 3.4 The boundary conditions of the plate theory

The necessary boundary conditions must be given along the outer boundary line $\partial\omega_0 \subset \Gamma_0$, and along the contact line $S_0$ between the wafer and the support ring.

We obtain the 2D boundary conditions along boundary line $\partial\omega_0$ from the 3D boundary conditions on $\Gamma_0$, (17) through (25), by the requirement, that the 3D conditions must only be satisfied in the mean. In other words they follow by integration of the 3D boundary conditions over the thickness of the plate.

Along $\partial\omega_0$ there are five resultants $N^{nn}$, $N^{sn}$, $M^{nn}$, $M^{sn}$ and $Q^n$, respectively, where we have used the abbreviations $N^{nn} = N_{\alpha\beta} n_\alpha n_\beta, N^{sn} = N_{\alpha\beta} s_\alpha n_\beta, M^{nn} = M_{\alpha\beta} n_\alpha n_\beta, M^{sn} = M_{\alpha\beta} s_\alpha n_\beta, Q^n = Q_\alpha n_\alpha, \boldsymbol{n} = (n_1, n_2, 0)$ and $\boldsymbol{s} = (-n_2, n_1, 0)$ denote the normal vector and the tangent vector, respectively, on $\partial\omega_0$.

The 2D versions of the 3D boundary conditions read

$$N^{nn} = 0 \quad \text{along} \quad \partial\omega_0, \tag{49}$$

$$N^{sn} = 0 \quad \text{along} \quad \partial\omega_0 \quad \text{except in} \quad P_{0O}, P_{0N}, P_{0W}, \tag{50}$$

$$M^{nn} = 0 \quad \text{along} \quad \partial\omega_0 \quad \text{and} \tag{51}$$

$$U_\alpha s_\alpha = 0 \quad \text{in} \quad P_{0O}, P_{0N}, P_{0W}. \tag{52}$$

Herein $P_{0O}, P_{0N}$ and $P_{0W}$ indicate the locations, where rigid body motions of the plate are prevented, see (16).

Furthermore we require

$$Q^n + \frac{\partial M^{ns}}{\partial s} + N^{nn}\frac{\partial W}{\partial n} + N^{ns}\frac{\partial W}{\partial s} = 0 \quad \text{along} \quad \partial\omega_0 \quad \text{with} \tag{53}$$

$$N^n_\alpha \frac{\partial W}{\partial X_\alpha} = N^n_1 \frac{\partial W}{\partial X_1} + N^n_2 \frac{\partial W}{\partial X_2} = N^{nn}\frac{\partial W}{\partial n} + N^{ns}\frac{\partial W}{\partial s},$$

where $s$ gives the curve parameter along $\partial\omega_0$.

***Remark:*** The three 2D boundary conditions (49) through (51) result directly by integration of (17) and (20), while the condition (53) requires a different reasoning. The three 2D boundary conditions (17) and (20) cannot be supplemented by the additional prescription of $M^{sn}$ and $N^n_\alpha \frac{\partial W}{\partial X_\alpha}$ along $\partial\omega_0$, because we were then confronted with five conditions instead of only four boundary conditions that are needed. For this reason both quantities must be adequately combined to a single one. This cannot be done arbitrarily, and already *Kirchhoff* recognized this fact in the year 1850. He showed within the framework of his linear plate theory that the prescription of the quantity gives the necessary fourth boundary condition. This result follows naturally from the weak formulation of the plate equations, which, however, are not given in this paper, see [5] for details. If we follow the strategy, which was given by *Kirchhoff*, we may also deduce the additional boundary condition (53) from the weak formulation of the *von Kármán* plate theory, see again [5] for details.

The boundary condition (52) on $S_0$, which is specified in (15), yields now the condition

$$W = 0 \quad \text{on} \quad S_{00} \quad \text{with} \tag{54}$$

$$S_{00} = \{(X_1, X_2) | (X_1 + U_1(X_1, X_2))^2 + (X_2 + U_2(X_1, X_2))^2 = R_I^2\} \subset \omega_0.$$

This is a free boundary condition, because the locations of the line $S_{00}$ depend on the $U_\alpha$, which is part of the solution. Since there holds $|U_\alpha| \ll h \ll R_I$, the line $S_{00}$ may be approximated by a line $S_{00V}$ , that does not depend on $U_\alpha$, so that we obtain the explicit boundary

$$W = 0 \quad \text{on} \quad S_{00V} \quad \text{with} \quad S_{00V} = \{(X_1, X_2) | X_1^2 + X_2^2 = R_I^2\} \subset \omega_0. \tag{55}$$

Thus there is now a complete set of boundary conditions, so that the fields of displacements are uniquely determined. The calculation of the stresses will be done in a subsequent step, which is explained in the next subsection.

## 3.5 Stress calculation within the *von Kármán* plate theory

The now known displacement fields $U_\alpha$ and $W$ yield the stress resultants and couples $N_{\alpha\beta}$, $M_{\alpha\beta}$ and $Q_{\alpha\beta}$, and if these are sufficiently smooth, we may also calculate their with respect to $X_1$ and $X_2$. The exploitation of the 2D constitutive law (35) yields by means of (47) and (48) to the relation

$$\sigma_{\alpha\beta}(X_1, X_2, X_3) = \frac{1}{h} N_{\alpha\beta}(X_1, X_2) + \frac{12 X_3}{h^3} M_{\alpha\beta}(X_1, X_2). \tag{56}$$

and the remaining stresses follow by exploitation of the equilibrium condition (37) and the boundary conditions for various stresses viz. (17), (18), and (20) through (24). We obtain

$$\frac{1}{h}\frac{\partial N_{\alpha\beta}}{\partial X_\beta}+\frac{12X_3}{h^3}\frac{\partial M_{\alpha\beta}}{\partial X_\beta}+\frac{\partial \sigma_{\alpha 3}}{\partial X_3}=0 \quad \text{and} \quad \frac{\partial}{\partial X_\beta}\left(\sigma_{3\beta}+\frac{\partial W}{\partial X_\alpha}\sigma_{\alpha\beta}\right)+\frac{\partial T_{33}}{\partial X_3}=0. \tag{57}$$

The left equation of (57) and the boundary conditions (21) and (22) yield

$$\sigma_{\alpha 3}(X_1,X_2,X_3)=\frac{6}{h^3}\left(\frac{h^2}{4}-X_3^2\right)\frac{\partial M_{\alpha\beta}(X_1,X_2)}{\partial X_\beta}, \tag{58}$$

while the third equation of (57) gives the differential equation

$$\frac{6}{h^3}\left(\frac{h^2}{4}-X_3^2\right)\frac{\partial^2 M_{\alpha\beta}}{\partial X_\alpha \partial X_\beta}+\frac{\partial^2 W}{\partial X_\alpha \partial X_\beta}\left(\frac{1}{h}N_{\alpha\beta}+\frac{12X_3}{h^3}M_{\alpha\beta}\right) + \frac{12X_3}{h^3}\frac{\partial W}{\partial X_\alpha}\frac{\partial M_{\alpha\beta}}{\partial X_\beta}+\frac{\partial T_{33}}{\partial X_3}=0.$$

After its integration we obtain

$$\begin{aligned} T_{33}(X_1,X_2,X_3)= \quad & -\frac{\partial^2 W(X_1,X_2)}{\partial X_\alpha \partial X_\beta}X_3\left(\frac{1}{h}N_{\alpha\beta}(X_1,X_2)+\frac{6X_3}{h^3}M_{\alpha\beta}(X_1,X_2)\right) \\ & -X_3\frac{6}{h^3}\left(\frac{h^2}{4}-\frac{1}{3}X_3^2\right)\frac{\partial^2 M_{\alpha\beta}(X_1,X_2)}{\partial X_\alpha \partial X_\beta} \\ & -\frac{6X_3^2}{h^3}\frac{\partial W(X_1,X_2)}{\partial X_\alpha}\frac{\partial M_{\alpha\beta}(X_1,X_2)}{\partial X_\beta}+C(X_1,X_2), \end{aligned}$$

so that we finally obtain with $\sigma_{33}=T_{33}-\frac{\partial W}{\partial X_\alpha}\sigma_{\alpha 3}$ the representation

$$\begin{aligned} \sigma_{33}(X_1,X_2,X_3)= \quad & -\frac{\partial^2 W(X_1,X_2)}{\partial X_\alpha \partial X_\beta}X_3\left(\frac{1}{h}N_{\alpha\beta}(X_1,X_2)+\frac{6X_3}{h^3}M_{\alpha\beta}(X_1,X_2)\right) \\ & -X_3\frac{6}{h^3}\left(\frac{h^2}{4}-\frac{1}{3}X_3^2\right)\frac{\partial^2 M_{\alpha\beta}(X_1,X_2)}{\partial X_\alpha \partial X_\beta} \\ & -\frac{3}{2h}\frac{\partial W(X_1,X_2)}{\partial X_\alpha}\frac{\partial M_{\alpha\beta}(X_1,X_2)}{\partial X_\beta}+C(X_1,X_2). \end{aligned}$$

Next we eliminate by means of (44) the stress resultants $N_{\alpha\beta}$ and obtain

$$\begin{aligned} &\sigma_{33}(X_1,X_2,X_3) \\ &\quad =\left(\left(\frac{h^2}{4}-X_3^2\right)N_{\alpha\beta}(X_1,X_2)-3X_3M_{\alpha\beta}(X_1,X_2)\right)\frac{2X_3}{h^3}\frac{\partial^2 W(X_1,X_2)}{\partial X_\alpha \partial X_\beta} \\ &\qquad -\frac{\partial W(X_1,X_2)}{\partial X_\alpha}\frac{3}{2h}\frac{\partial M_{\alpha\beta}(X_1,X_2)}{\partial X_\beta}+\frac{2X_3}{h^3}\left(\frac{3h^2}{4}-X_3^2\right)p(X_1,X_2) \\ &\qquad\qquad +C(X_1,X_2). \end{aligned}$$

For the determination of the function $C(X_1, X_2)$ we exploit the boundary conditions (23) or (24), and obtain with $C(X_1, X_2) = \frac{\partial W(X_1,X_2)}{\partial X_\alpha} \frac{3}{2h} \frac{\partial M_{\alpha\beta}(X_1,X_2)}{\partial X_\beta} - \frac{p(X_1,X_2)}{2} + \frac{\partial^2 W(X_1,X_2)}{\partial X_\alpha \partial X_\beta} \frac{3}{2h} M_{\alpha\beta}(X_1, X_2)$ the 33-component of the stress according to

$$\begin{aligned}
&\sigma_{33}(X_1, X_2, X_3) \\
&\quad = \left(\frac{h^2}{4} - X_3^2\right) \frac{2}{h^3} \big(X_3 N_{\alpha\beta}(X_1, X_2) + 3M_{\alpha\beta}(X_1, X_2)\big) \frac{\partial^2 W(X_1, X_2)}{\partial X_\alpha \partial X_\beta} \\
&\qquad + \left(\frac{2X_3}{h^3}\left(\frac{3h^2}{4} - X_3^2\right) - \frac{1}{2}\right) p(X_1, X_2) \\
&\qquad\qquad \text{on} \quad \Omega^0 \quad \text{except on} \quad S_{00V} \times [-h/2, h/2]. \quad (59)
\end{aligned}$$

# 4 Calculation of the external pressure and the contact surface between the load sphere and the plate

According to the theory of *Hertz*, we now calculate the shape and the size of the contact area $K \subset \Omega_{0-}$ of the load-sphere / plate system and the pressure distribution on $K$. To this end we assume that the contact problem for a sphere and an infinite half-space is an approximate model. This problem was posed and solved already in the year 1881 by *Heinrich Hertz*.

The result reads: An isotropic steel sphere, with radius $R_S$, *Young* modulus $E_S$ and *Poisson* ratio $\nu_S$, in contact with an isotropic half space with elastic constants $E$ and $\nu$ induces due to an external force $f$ a contact surface with radius

$$R_K = \sqrt[3]{3/4 \; f \; R_S \; k} \quad \text{with} \quad k = \frac{1 - \nu_S^2}{E_S} + \frac{1 - \nu^2}{E}. \tag{60}$$

The pressure distribution on the contact surface is given by

$$p^f(r) = p_0^f \sqrt{1 - (r/R_K)^2} \quad \text{with} \quad p_0^f = \frac{3f}{2\pi R_K^2}, \; r = \sqrt{X_1^2 + X_2^2}, \tag{61}$$

so that

$$\iint\limits_{\partial\Omega^f} p^f\,(r(X_1, X_2))\mathrm{d}X_1\mathrm{d}X_2 = f \quad \text{and} \quad p_0^f = \frac{1}{I}\sqrt[3]{\frac{48f}{R_K^2}} \quad \text{with} \quad I = 2\pi \; k^{\frac{2}{3}}, \tag{62}$$

respectively.

This result was extended by *Willis* [14] to an isotropic sphere, which in contact with a material of cubic symmetry. However, *Willis* only allows ellipses as the boundary of the contact area, and concluded that the boundary of the contact area must be a circle.

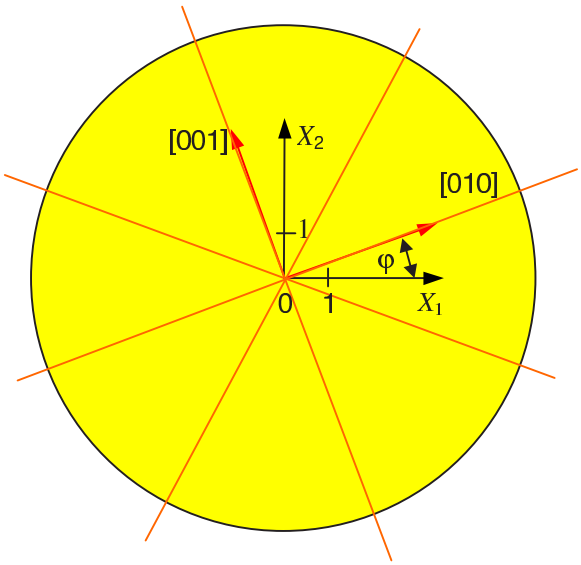


Figure 2: The main frame of the crystal is rotated in the (100)-plane by the angel $\varphi$. The thin lines represents the symmetry of the cubic material.

We proceed differently as follows: We start our calculation of the *Hertz* relations from the equations (60) through (62) . However, we take into account for a material with cubic symmetry, that the effective Young modulus and the effective Poisson ration must be depend on a direction.

In the case at hand, only rotations with respect to the $X_3$-axis must be considered, and the rotation matrix thus reads

$$\boldsymbol{Q} = \begin{pmatrix} \cos(\varphi) & -\sin(\varphi) & 0 \\ \sin(\varphi) & \cos(\varphi) & 0 \\ 0 & 0 & 1 \end{pmatrix} \tag{63}$$

The compliance tensor $S_{ijmn}$ (13), which is originally given with respect to a coordinate frame that coincides with the crystal axes can by means of (63) calculated in a frame whose $X_1$- and $X_2$- axis does not coincide with the crystal axes. We denote the components of the compliance with respect to a frame whose $X_1$- and $X_2$- axis are rotated against the crystal axes by the angle $\varphi$ with $S_{ijmn}(\varphi)$, and we note the relation

$$S_{ijkl}(\varphi) = Q_{im}Q_{jn}Q_{kp}Q_{lq}S_{mnpq}. \tag{64}$$

which is used to identify the angle- dependent *Young* modulus and *Poisson* ratio according to the representation:

$$\begin{aligned} \frac{1}{E(\varphi)} &= S_{1111}(\varphi) = Q_{1m}Q_{1n}Q_{1p}Q_{1q}s_{mnpq} = s_{11} - 2\left(s_{11} - s_{12} - \frac{s_{44}}{2}\right)Q_{11}^2Q_{12}^2 \\ &= s_{11} - \frac{1}{2}\left(s_{11} - s_{12} - \frac{s_{44}}{2}\right)\sin^2(2\varphi) \end{aligned} \tag{65}$$

and

$$\begin{aligned}\nu(\varphi) = -E(\varphi)\ s_{1122}(\varphi) &= -E(\varphi)\ Q_{1m}Q_{1n}Q_{2p}Q_{2q}s_{mnpq} \\ &= -E(\varphi)\left(s_{12} + \frac{1}{2}\left(s_{11} - s_{12} - \frac{s_{44}}{2}\right)\sin^2(2\varphi)\right).\end{aligned} \tag{66}$$

In an analogous manner we obtain the angle dependent contact

$$R_K(\varphi) = \sqrt[3]{3/4\ f\ R_S\ k(\varphi)} \quad \text{with} \quad k(\varphi) = \frac{1-\nu_S^2}{E_S} + \frac{1-(\nu(\varphi))^2}{E(\varphi)}. \tag{67}$$

The Figure 3 shows the shape of the boundary of the contact surface for a given force $f = 100$ N. Additionally, Figure 3 shows a circle, which gives the boundary of the contact surface according to an iso-tropic mean according to the *Reuss* rule.

The anisotropic pressure distribution on the contact surface reads analogously to (61)

$$p(r,\varphi) = p_0\sqrt{1-(r/R_K(\varphi))^2}. \tag{68}$$

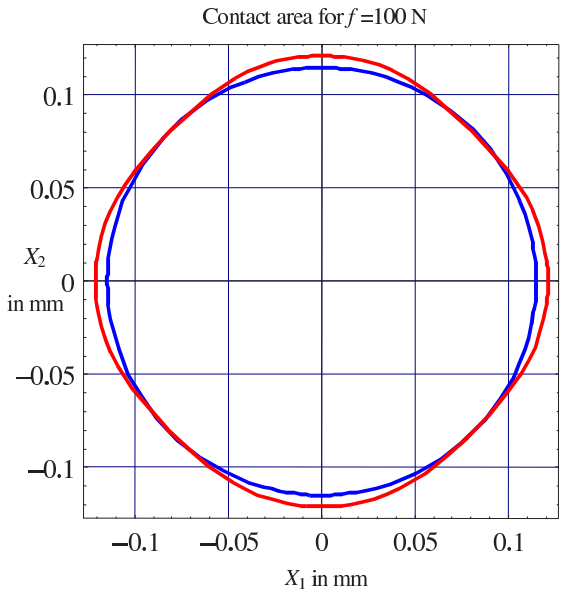


Figure 3: Contact area of the sphere-wafer-system. Outer curve: cubic symmetry. Inner circle: an isotropic mean according to the *Reuss* rule.

The calculation of $p_0$ in (68) needs the exploitation of

$$\iint_K p(r(X_1,X_2),\varphi(X_1,X_2))\ \mathrm{d}X_1\ \mathrm{d}X_2 = f$$

| force in N | radius in mm ⟨100⟩ | ⟨110⟩ | force in N | radius in mm ⟨100⟩ | ⟨110⟩ |
|---|---|---|---|---|---|
| 50 | 0.09607 | 0.09076 | 300 | 0.17458 | 0.16492 |
| 100 | 0.12104 | 0.11435 | 350 | 0.18378 | 0.17362 |
| 150 | 0.13856 | 0.13090 | 400 | 0.19215 | 0.18152 |
| 200 | 0.15251 | 0.14407 | 450 | 0.19984 | 0.18879 |
| 250 | 0.16428 | 0.15520 | | | |

Table 1: Contact radii as a function of the pressure force and the orientation of the single crystal.

by means of the angle dependent contact radius according to (64). There results analogously (62)

$$p_0 = \frac{1}{I}\sqrt[3]{\frac{48f}{R_K^2}} \quad \text{mit} \quad I = 8\int_0^{\pi/4} (k(\varphi))^{\frac{2}{3}}\,\mathrm{d}\varphi. \tag{69}$$

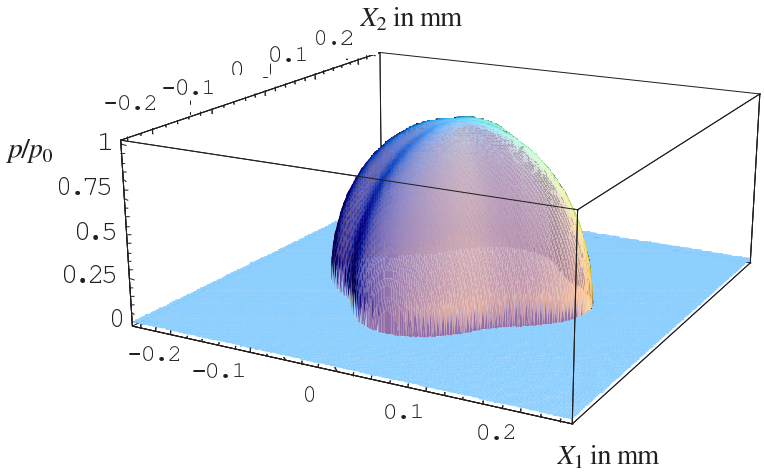


Figure 4: Pressure distribution on the contact surface.

We conclude from the figures 3 and 4 that there is only a weak anisotropy in GaAs.

# 5 Some remarks on the weak formulation of the *von Kármán* plate theory and its Finite-Element approximation

In the following we deduce the weak formulation of the three equations $(41)_{1,2}$ and (44) for the displacements of the middle surface $U_a$ and $W$, which form the basis for Finite-Element formulations.

To this end we introduce sufficiently smooth test function $V_i(X_1, X_2),\ i \in 1, 2, 3.$ The boundary condition (52) fort he displacement implies that the components $V_\alpha(X_1, X_2),\ \alpha \in 1, 2$ must vanish in the horizontal rigid body bond points (16)

$$V_\alpha s_\alpha = 0 \quad \text{in} \quad P_{0O}, P_{0N}, P_{0W}. \tag{70}$$

Furthermore, according (55), the third component $V_3$ must vanish along the trust line:

$$V_3 = 0 \quad \text{along} \quad S_{00V}. \tag{71}$$

Next we multiply the membrane equations (41) with $V_\alpha$ and hereafter we integrate on the middle surface $\omega_0$ of the plate to obtain

$$\iint\limits_{\omega_0} \frac{\partial N_{\alpha\beta}}{\partial X_\beta} V_\alpha \, \mathrm{d}X_1 \mathrm{d}X_2 = 0. \tag{72}$$

After partial integration we obtain by means of the boundary conditions (49) and (50)

$$\iint\limits_{\omega_0} N_{\alpha\beta} \frac{\partial V_\alpha}{\partial X_\beta} \, \mathrm{d}X_1 \mathrm{d}X_2 = 0. \tag{73}$$

Analogously we multiply the equation (44) with $V_3$ and integrate again on the middle surface w of the plate. There results

$$\iint\limits_{\omega_0} \left( \frac{\partial}{\partial X_\alpha} \left( Q_\alpha + N_{\alpha\beta} \frac{\partial W}{\partial X_\beta} \right) + p \right) V_3 \, \mathrm{d}X_1 \mathrm{d}X_2 = 0. \tag{74}$$

Partial integration of (74) and the equation (43) yield

$$\begin{aligned} \iint\limits_{\omega_0} \left( \frac{\partial M_{\alpha\beta}}{\partial X_\beta} + N_{\alpha\beta} \frac{\partial W}{\partial X_\beta} \right) \frac{\partial V_3}{\partial X_\alpha} \, \mathrm{d}X_1 \mathrm{d}X_2 \\ = \int\limits_{\partial\omega_0} \left( Q_\alpha + N_{\alpha\beta} \frac{\partial W}{\partial X_\beta} \right) V_3 \, n_\alpha \, \mathrm{d}s + \iint\limits_{\omega_0} p \, V_3 \, \mathrm{d}X_1 \mathrm{d}X_2. \end{aligned} \tag{75}$$

A further partial integration of the left hand side of (75) gives rise to the following consequence of (75)

$$\begin{aligned}
&\iint\limits_{\omega_0} \left( N_{\alpha\beta} \frac{\partial W}{\partial X_\beta} \frac{\partial V_3}{\partial X_\alpha} - M_{\alpha\beta} \frac{\partial^2 V_3}{\partial X_\alpha \partial X_\beta} \right) \mathrm{d}X_1 \mathrm{d}X_2 \\
&\quad = \int\limits_{\partial\omega_0} \left( \left( Q_\alpha + N_{\alpha\beta} \frac{\partial W}{\partial X_\beta} \right) V_3 - M_{\alpha\beta} \frac{\partial V_3}{\partial X_\beta} \right) n_\alpha \, \mathrm{d}s + \int\limits_{\omega_0} p \, V_3 \, \mathrm{d}X_1 \mathrm{d}X_2 \\
&\quad = \int\limits_{\partial\omega_0} \left( \left( Q^n + N^n_\beta \frac{\partial W}{\partial X_\beta} \right) V_3 - M^{ns} \frac{\partial V_3}{\partial s} - M^{nn} \frac{\partial V_3}{\partial n} \right) \mathrm{d}s + \int\limits_{\omega_0} p \, V_3 \, \mathrm{d}X_1 \mathrm{d}X_2.
\end{aligned}$$

Now we recall that the moments and the resultants vanish according (51) and (53) on the boundary $\partial\omega_0$, so that we finally obtain

$$\iint\limits_{\omega_0} \left( N_{\alpha\beta} \frac{\partial W}{\partial X_\beta} \frac{\partial V_3}{\partial X_\alpha} - M_{\alpha\beta} \frac{\partial^2 V_3}{\partial X_\alpha \partial X_\beta} \right) \mathrm{d}X_1 \mathrm{d}X_2 = \int\limits_{\omega_0} p \, V_3 \, \mathrm{d}X_1 \mathrm{d}X_2. \tag{76}$$

The equations (73) and (76) and the boundary conditions (52) and (55) yield a coupled system for the functions $U_\alpha$ und $W$, which generate weak solutions of the original boundary value problem for all admissible test functions $V_i$. Approximative weak solutions follow from Finite-Element discretisations of this system , if we assume that (73), (76) and (52), (55) must only hold for a finite subset of all admissible test functions $V_i$. In other words: For $N$ independent test functions we approximate the displacements by ansatz-functions, which are fully characterized by $N$ independent parameter. The objective of the Finite-Element method is the determination of these parameters. The details of the used ansatz- and test- functions and their subsequent exploitation are found in the thesis [5].

# 6 Numerical Results

## 6.1 Test regarding the numerical accuracy of plate elements

At first we check the performance of the used finite elements code. To this end we compare well known analytical solutions with their approximations. As a test example we choose an isotropic circular plate, whose outer boundary is simply supported, and which can be described by the Kirchhoff plate theory. The following figure shows the flexure that is induced by a concentric point load which corresponds to the force $f = 1$ N. The curve represents the analytical solution, while the dots result from the Finite-Element approximation. Both solutions coincide up to at least four digits, which exhibits the high quality of the approximation.

The used Finite Element mesh is shown in Figure 6. We can seen, that we use in contact area and in the vicinity of of the plate boundary a very fine mesh.

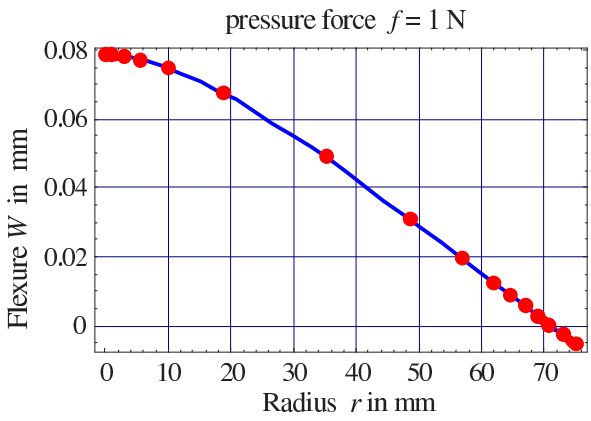


Figure 5: Comparison of an analytical solution according to *Kirchhoff* (line) and the corresponding Finite-Element solution (dots) for a cental point load.

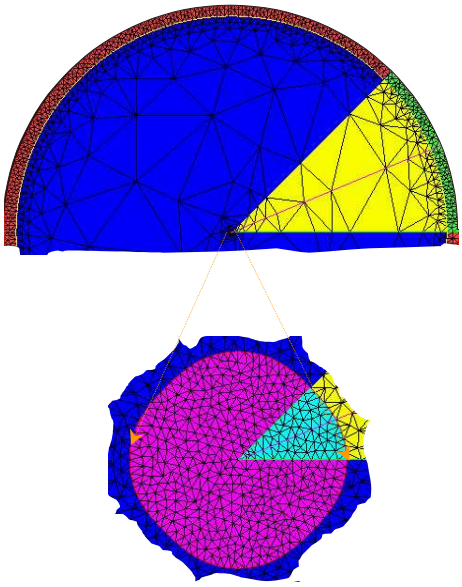

Figure 6: Mesh of whole circle for the 2D plate problem with special marked area for the post process analysis. Top: Upper half of the full mesh. Down: Mesh of the contact area with a zoom factor of 350.

## 6.2 Numerical results versus experiment

The only possibility to test the validity of the modelling assumptions and their numerical implementation is a comparison of calculated and experimental load-flexure curves, which give the dependence of the maximal displacement $W$ on the applied load $f$.

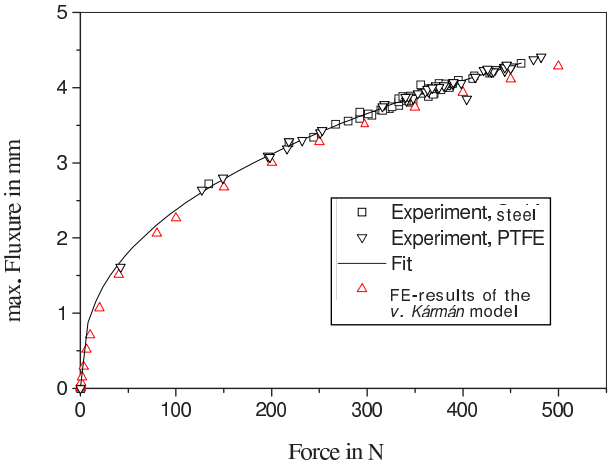


Figure 7: Comparison of maximal displacements, theory vs. experiment, for a wafer with diameter 150 mm.

We compare in Figure 7 the experimental load-flexure relations with the results according to the FE discretisation of the model that is described in Sections 3 and 4. The geometric data of the considered wafer are given in Section 1.3. The experiments are carried out for two different load spheres made from steel and teflon (PFTE), respectively. We observe the following facts: (*i*) The experimental data do satisfactorily agree with the numerical data. (*ii*) The numerical wafer, however, behaves somewhat more stiff as the experimental wafer, if we exclude experimental errors. The maximal deviations between experimental and numerical data are 4%. The calculated data can be read off from the Table 2. (*iii*) The experimental load-flexure relations do not depend on the material of the load sphere.

The exploitation of the experimental data give also important hints regarding the modelling assumptions. 1. The load-flexure relations exhibit an apparently nonlinear behaviour. This cannot be described within the framework of a linear plate theory, which always predict a linear load-flexure dependence. Consequently, the linear model is not applicable for the considered load range. 2. The boundary conditions (22) that were formulated in Section 2.4 rely on the assumption that the wafer may slip without friction on the support ring. This is not an obvious assumption, rather it is motivated by the experimental data. The alternative assumption were that the wafer does not slip on the support ring is excluded by the experimental data, because in this case the calculated displacements are by far too small in comparison with the experimental displacements. The details can be read off from Figure 8 which also contains the load-flexure dependence according to the (linear)

Kirchhoff theory.

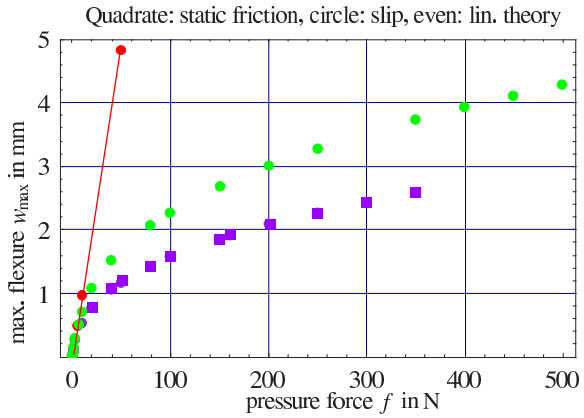


Figure 8: Comparison of maximal displacements for two different boundary conditions: points: slip is allowed, squares: no slip. The linear dependence results from the (linear) *Kirchhoff* theory.

## 6.3 Stress fields with anisotropic effects

In this section we consider a plate subjected to the load $f = 100$ N, and study the dependence of the radial stress $\sigma_{rr}$, the tangential stress $\sigma_{\varphi\varphi}$, and the torsion shear stress $\sigma_{r\varphi}$, on three rotation angels, viz. $\varphi = 0°, 22.5°, 45°$, with respect to the $\langle 100 \rangle$-crystal axes. The angle $\varphi$ is defined according to the figure 2. The radial as well as

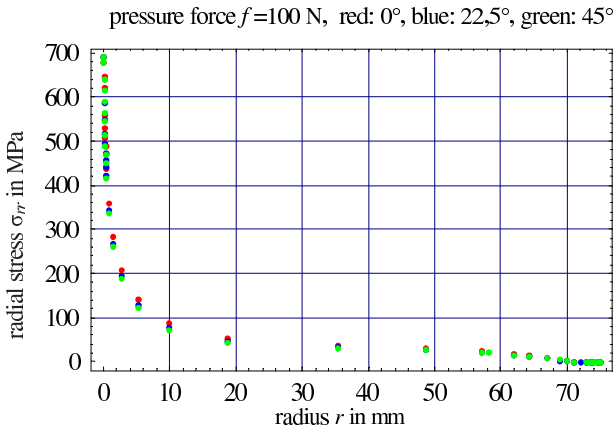


Figure 9: Radial stress / radius dependence at the lower plate surface $X_3 = h/2$ for three angels of orientation and the load $f = 100$ N.

the tangential stresses in figure 9 and figure 10 increase monotonously for decreasing radius. Their anisotropic contributions are small in GaAs. Let us now consider the radial stress in the vicinity of the center of the plate. We observe in figure 11 that the radial stress has an inflection point within the interval $0.113 \text{ mm} < r < 0.122$

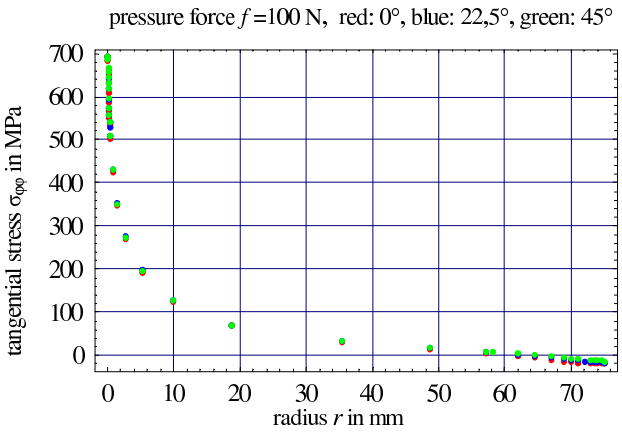


Figure 10: Tangential stress / radius dependence at the lower plate surface $X_3 = h/2$ for three angels of orientation and the load $f = 100$ N.

mm and assumes its maximum at $r = 0$. The values of the angle dependent contact radius can be read of from the table 1 on page 18. The torsion- shear stress $\sigma_{r\varphi}$

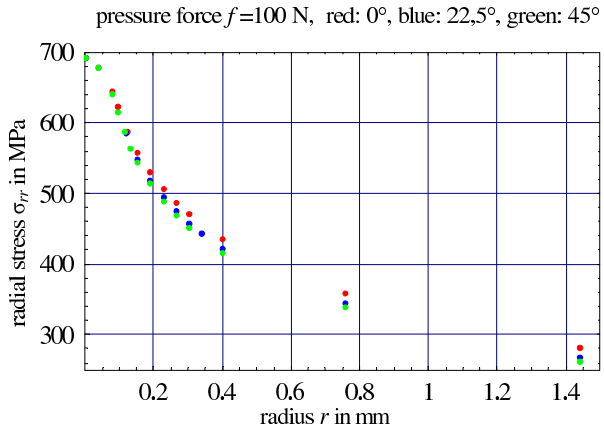


Figure 11: Radial stress / radius dependence at the lower plate surface $X_3 = h/2$ for three angels of orientation and the load $f = 100$ N. Note the different scale with respect to Figure 9.

results exclusively from the anisotropy of GaAs, because $\sigma_{r\varphi}$ vanishes identically for an isotropic material. Note that $\sigma_{r\varphi} = 0$ at $\varphi = 0°$, i.e. along the $\langle 100 \rangle$-axes. The maximal values of the torsion- shear stress reach at most 4 of the maximal values of tangential and radial stresses, and this happens at the boundary of the contact surface.

It is important to note that the stresses can not be measured, so that we can test the appropriateness of the calculated displacements only by the load-flexure dependence. However, if all the assumptions of Sections 3.1 and 3.2 for the passage from the 3D-model to the 2D-model are met in the experiment, a correct calculate load-flexure dependence might motivate that the stresses are also correctly calculated.

A careful study of the reported results reveal that the conditions on the displace-

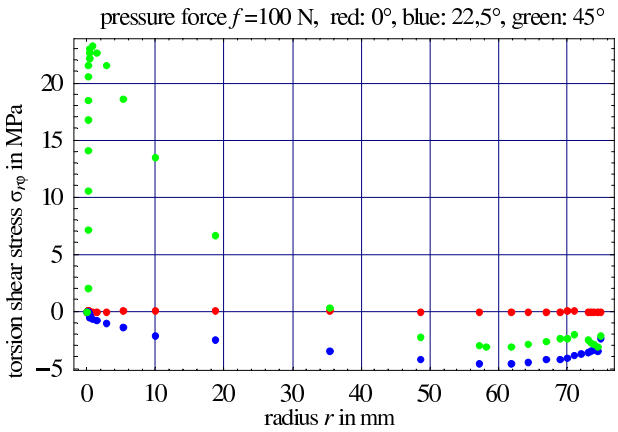


Figure 12: Torsion shear stress / radius dependence at the lower plate surface $X_3 = h/2$ for three angels of orientation and the load $f = 100$ N.

| $f$ in N | $w(0,0,X_3)$ in mm | $\sigma_{rr}(0,0,\frac{h}{2})$ in MPa | $\sigma_{rr}(0,0,-\frac{h}{2})$ in MPa | $\sigma_{33}(0,0,-\frac{h}{2})$ in MPa |
|---|---|---|---|---|
| 50 | 1.670 | 383.3 | -328.6 | -2719 |
| 100 | 2.584 | 691.6 | -580.5 | -3426 |
| 150 | 2.668 | 972.5 | -805.6 | -3921 |
| 200 | 2.994 | 1237 | -1014 | -4316 |
| 250 | 3.269 | 1488 | -1209 | -4649 |
| 300 | 3.510 | 1729 | -1395 | -4940 |
| 350 | 3.725 | 1962 | -1572 | -5201 |
| 400 | 3.920 | 2188 | -1742 | -5438 |
| 450 | 4.100 | 2406 | -1904 | -5655 |

Table 2: Maximal stresses and maximal displacements as functions of the load $f$ at $(X_1, X_2, X_3) = (0, 0, \pm h/2)$. For all $f$ there holds $\sigma_{33}(0,0,\frac{h}{2}) = \sigma_{r3}(0,0,\pm\frac{h}{2}) = 0$.

ments, viz. $|u_\alpha| \ll |u_3| \ll R_I$, are satisfied, while the conditions on the stresses, viz. $|\sigma_{33}| \ll |\sigma_{3\alpha}| \ll \|\sigma_{\alpha\beta}\|$, are only satisfied in the range $X_1^2 + X_2^2 > (5h)^2$. For $X_1^2 + X_2^2 < (\rho h)^2$ both inequalities are only satisfied in the vicinity of the lower plate surface $X_3 = h/2$. The maximal contradiction to the inequalities arises at the point $(X_1, X_2, X_3) = (0, 0, -h/2)$. In particular we have here $\sigma_{r3} = 0$.The other corresponding values of the stresses are given in Table 2.

We observe that the basic assumption of the plate theory are violated at $(X_1, X_2, X_3) = (0, 0, -h/2)$. Thus the calculated stresses are not correct in the vicinity of that point. Furthermore we observe that the violation of the stress conditions is larger for smaller loads as for larger loads, because the contact surface increases super-proportional with the load. However, the principle of *Saint-Venant* [12] guarantees, that this has no influence to the calculated stresses outside of that region.

If we were interested in the correct stresses also in the vicinity of $(X_1, X_2) = (0, 0)$

and $X_3 \in [-h/2, h/2]$, we have to calculate the stresses here by means of the 3D theory. A detailed analysis of this subtle problem was carried out by *F. Duderstadt* in his thesis [5]. It is shown that a linear 3D theory is sufficient to calculatet those stresses that cannot be obtained from a 2D theory, so that the stresses are given by analytic solutions. For example, for a load $f$=450 N, the maximal tensile stress at $(0, 0, X_3 = h/2)$ is approximately 4% smaller as the stress that results at this point from the 2D theory.

# References


[1] F. Bergner, U. Bergmann, R. Hammer, M. Jurisch und M. Schaper, *Mikro- und Ultramikrohärteprüfung an GaAs-Einkristallen*, Materialprüfung **43** (2001), no. 4, 117–122.

[2] C. P. Chen and M. H. Leipold, *Fracture thoughness of silicon*, Bull. Amer. Ceramic Soc. **59** (1980), 469.

[3] P. G. Ciarlet, *Mathematical elasticity,* vol. II, *Theory of Plates*, Studies in Mathematics and its Applications, no. 27, Elsevier, Amsterdam, 1997.

[4] E. and F. Cosserat, *Theorie des Corps Deformables*, A. Hermann et Fils, Paris, 1909.

[5] F. Duderstadt, *Anwendung der von Kármán'schen Plattentheorie und der Hertz'schen Pressung für die Spannungsanalyse zur Biegung von GaAs-Wafern im modifizierten Doppelringtest*, Ph.D. thesis, Technical University Berlin, 2003, also published as WIAS-Report, no. 24, URL `http://www.wias-berlin.de/publications/reports/24/`.

[6] S. M. Hu, *Critical stress in silicon brittle fracture, and effect of ion implantation and other surface treatments*, J. Appl. Phys. **53** (1982), no. 5, 3576–3580.

[7] Th. von Kármán, *Festigkeitsprobleme im Maschinenbau* (1910), Encyklopädie der mathematischen Wissenschaften (F. Klein und C. Müller, ed.), vol. IV/4, Teubner, Leipzig, 1907-1914, pp. 314–386.

[8] R. R. Mindlin, *Influence of rotatory inertia and shear on flexural motions of isotropic elastic plate*, J. Appl. Mech. **18** (1951), 31–38.

[9] NORM EN DIN 1288-5, *Glass in building — Determination of the bending strengh of glass — Part 5: Coaxial double ring test on flat specimens with small test surface areas*, 2000, replacement for DIN 52292-1.

[10] E. Willis, *The effect of transverse sher deformations on the bending of elastic plates*, J. Math. Phys. **23** (1945), 184–191.

[11] C. Truesdell and W. Noll, *The non-linear field theories of mechanics*, Springer, Berlin, 1965, 1. Editon (1965) in *Encyclopadia of Physics* (vol. III/3), 2. corrected Edition (1992).

[12] C. Truesdell and Toupin R., *The classical field theories*, Prinzipien der klassischen Mechanik und Feldtheorie (S. Flüge, ed.), Handbuch der Physik, vol. III/1, Springer, Berlin, 1960, pp. 226–793.

[13] M. S. Wdowik, *Reduction of wafer breakage in a* 3″ *wafer fab facility through the implementation of a biaxial stress test*, US Conf. on GaAs Manufacturing (Reno), June 1990.

[14] J. R. Willis, *Hertzian contact of anisotropic bodies*, Journal of the Mechanics and the Physics of Solids **14** (1966), 163–176.